Integrated geophysical characterization of crustal domains in the Eastern Black Sea

Vanessa Monteleone[1, 2], Tim A. Minshull[1], and Hector Marin-Moreno[2]

[1]School of Ocean and Earth Science, University of Southampton, National Oceanography Centre Southampton, Waterfront Campus, European Way, Southampton SO14 3ZH, UK (v.monteleone@soton.ac.uk; tmin@noc.soton.ac.uk).

[2]National Oceanography Centre, University of Southampton Waterfront Campus, European Way, Southampton SO14 3ZH, UK (hector.marin.moreno@noc.ac.uk).

ABSTRACT

Rifting may lead ultimately to continental breakup, but the identification and characterization of the resulting crustal distribution remains challenging. Also, spatial and temporal changes in breakup magmatism may affect the geophysical character of the newly formed oceanic crust, resulting in contrasting interpretations of crustal composition and distribution. In the Eastern Black Sea Basin (EBSB), the evolution from rifting to breakup has been long debated, with several interpretations for the distribution of stretched continental and oceanic crust. We interpret basement morphological variations from long-offset seismic reflection profiles, highlighting a NW-SE transition from faulted and tilted continental blocks, to a rough and then smoother basement. We model magnetic anomalies to constrain further the various basement domains, and infer the presence of a weakly-magnetized, stretched continental crust in the NW, and a 0.4-2.8 A/m layer coinciding with the smooth basement in the central and SE area. We conclude that the EBSB oceanic crust extends further to the NW than was suggested

23 previously from an abrupt change in crustal thickness and lower-crustal velocity. The apparent
24 discrepancy between these different types of geophysical evidence may result from changes in
25 magma supply during breakup, affecting thickness and velocity structure of the resulting oceanic
26 crust.

27 ## 1. INTRODUCTION and METHOD

28 Observations of the structure and composition of the basement underlying rifted margins can
29 unravel the geodynamic processes driving their formation. High-quality, 2D/3D regional seismic
30 datasets provide insights into basement structures and sediment filling within the distal part of
31 the margin, thus helping geodynamic reconstruction (e.g., Tucholke et al., 2007; Haupert et al.,
32 2016). In deep-water and thick sedimentary infill settings, and when the basement is neither
33 exposed nor sampled by well data, our ability to interpret rifting and breakup features and
34 basement structures is limited. Particularly in these cases, refraction seismic (e.g., Dunn and
35 Martinez, 2011) and potential field data (e.g., Ball et al., 2013) can be used to investigate the
36 nature of the crust, its thickness and velocity structure, and the amount of magmatism
37 contributing at its formation (e.g., Franke, 2013). Only a few studies integrate these approaches
38 (e.g., Prada et al., 2014; Tugend et al., 2015).
39 In the Eastern Black Sea Basin (EBSB), interpretations of different datasets commonly disagree.
40 Crustal thickness and lower-crustal velocities from wide-angle seismic data define a small area
41 of oceanic crust to the SE of the basin (Shillington et al., 2009). Evidence for hummocky
42 basement structures along seismic reflection profiles suggest a narrow and elongated oceanic
43 crust extending further NW (Nikishin et al., 2015). Gravity modeling has also been used to
44 define crustal boundaries, with different results (e.g., Starostenko et al., 2004; Graham et al.,
45 2013) (Fig. DR1 in GSA Data Repository[1]). Therefore, although it is generally agreed that the

EBSB formed as a Late Cretaceous-early Cenozoic back-arc basin (e.g., Zonenshain and Le Pichon, 1986; Finetti et al., 1988; Okay et al., 1994), its crustal distribution is still debated. New long-offset seismic reflection profiles, acquired in 2011 by Geology Without Limits (GWL) and ION GXT (Table DR1), allowed Monteleone et al. (2019) to define the spatial and temporal distribution of extension and breakup processes in the EBSB. Here, we build on that analysis using additional data to untangle the lack of consensus on the EBSB crustal distribution. We first differentiate crustal domains based on basement morphological changes and the interaction between basement structures, stratigraphic and structural elements visible from long-offset seismic reflection profiles. We then apply magnetic anomaly modeling constrained by our seismic interpretation to investigate the magnetization character of the seismically identified domains, using the Earth Magnetic Anomaly Grid (EMAG2-v3) over the EBSB region (Meyer et al., 2017) (Fig. 1; Fig. DR2-8) (see GSA Data Repository). Magnetic data have been previously used in the Black Sea to define the age of basin opening (Kazmin et al., 2007), crustal scale structures and faulting (Starostenko et al., 2015), and the thermal structure of the lithosphere (Starostenko et al., 2014), but no modeling has been attempted yet to define crustal composition. Our results show a NW-SE change in morphological and magnetic character of the EBSB basement. Our inferred oceanic domain extends into a region where the presence of thinned continental crust was previously inferred from the seismic velocity structure. We relate our new interpretation to along-axis changes in breakup kinematics and magma supply during spreading.

2. RESULTS and DISCUSSION

2.1. Seismic Interpretation and Magnetic Anomaly Modeling

We identify the EBSB basement as the most continuous seismic reflection underlying the sedimentary infill, showing a variable morphological and structural character (Fig. 2). Over the structural highs (Shatsky Ridge and MBSH) and within the narrow NW rift, the basement is affected by normal faults generating half-graben structures bounded by faulted and tilted crustal blocks overlain by clear wedge-shaped syn-rift deposits (Fig. 2B). These elements are typically associated with stretched continental basement (Domain I) (Fig. 2A, 2B). In this area, the observed magnetic anomaly is best fit by a weakly-magnetized layer (< 0.4 A/m), also suggesting a continental nature for Domain I, bounded by two highly magnetized layers corresponding to mafic magmatism over the Shatsky Ridge and MBSH (e.g., Starostenko et al., 2004; Nikishin et al., 2015) (Fig. DR2-7). Previous results from wide-angle seismic data support this interpretation (Fig. 2A).

Seaward of Domain I, the basement has relief of similar magnitude but with no evidence for extensional faulting, nor clear syn-rift deposits (Fig. 2C). This basement extends 70-80 km along-axis, and from its distinctive morphological character we interpret it as a separate crustal domain (Domain II) (Fig. 2A, 2C). This rough basement was interpreted by Nikishin et al. (2015) as having oceanic affinity. Rough basement may result from slow seafloor spreading (e.g., Malinverno, 1991), or mantle exhumation processes (e.g., Sauter et al., 2018). The observed magnetic anomaly along Domain II is best fit by a weakly-magnetized layer, suggesting a continental rather than oceanic nature (Fig. 2C; Fig. DR4-5). Although we cannot rule out the presence of exhumed mantle, which also may have rather weak magnetization (e.g.,

87 Sibuet et al., 2007), seismic velocities suggest the presence of highly stretched continental crust
88 in this area (Shillington et al., 2009) (Fig. 2A).
89 The rough basement of Domain II becomes smoother towards the central and SE part of the
90 basin where well-layered, post-rift deposits are predominant (Domain III) (Fig. 2D, 2E; Fig.
91 DR4-7). No extensional faults are visible from seismic data, although high-angle NE-SW-
92 trending transform faults are present (Fig. 2A, 2E). Along some profiles, volcano-like structures
93 have been interpreted as evidence for enhanced magmatism in this area (Nikishin et al., 2015)
94 (Fig. 2A; Fig. DR7). Smooth basement with extrusive volcanic material may relate to
95 anomalously thick and/or fast spreading oceanic crust (e.g., Small, 1994; Searle et al., 2010),
96 exhumed mantle (e.g., Pickup et al., 1996), or thinned continental crust overlain by basaltic flows
97 (e.g., Zhao et al., 2016). At Domain III, magnetic anomaly data is best fit with negatively
98 magnetized layers with intensity bands between 0.4 and 2.8 A/m, in contrast to the weakly
99 magnetized Domain II (< 0.4 A/m) (Fig. 3; Fig. DR2), thus providing evidence against
100 continental crust or exhumed mantle. Serpentinized exhumed mantle may be significantly
101 magnetized (e.g., Sibuet et al., 2007), but its presence is excluded based on crustal seismic
102 velocities (Shillington et al., 2009).
103 Seismic data and magnetic anomaly modeling results support the presence of smooth and
104 magnetized oceanic crust along Domain III (Fig. 2-3; Fig. DR2-7). However, wide-angle data
105 indicate the presence of a thin crust (7-9 km) with low lower-crustal velocities (6.4-6.6 km/s) in
106 the NW, and of a thick crust (11-13 km) with high lower-crustal velocities (6.8-7.2 km /s) in the
107 SE. This change in crustal structure occurs close to the Ordu-Pitsunda transform fault (OPf) (Tari
108 et al., 2018), within Domain III (Fig. 2A, 2E). Shillington et al. (2009) interpreted this change as
109 a transition from highly stretched continental (NW) to thick oceanic (SE) crust (Fig. 2A), an

110 interpretation inconsistent with the uniform magnetization character of Domain III. Our results
111 show that the best-fitting model along profile bs-110, over crust interpreted as continental by
112 Shillington et al. (2009), is obtained with magnetizations of 2.4-3.2 A/m over the Shatsky Ridge
113 and 0.6 A/m towards the Pontides magmatic arc (Fig. 3; Fig. DR7). In the central basin, the
114 observed anomaly is best fit by a ~ 125 km wide, negatively magnetized layer, with intensity
115 bands between 0.4 and 2.4 A/m (Fig. 3; Fig. DR7). Similar results are obtained along profile bs-
116 100 at the NW end of Domain III, and profile bs-120 at the SE end of Domain III where the
117 velocity structure is clearly oceanic (Fig. 1, 2A; Fig. DR2-6). Although it is possible that
118 magnetic anomalies NW of the OPf are caused by syn-rift magmatic intrusions through thinned
119 continental crust (Starostenko et al., 2004), their intensity, overall continuity, and similarity to
120 anomalies in the oceanic domain to the SE, support their formation by seafloor spreading. Thus,
121 Domain III has a smooth and highly magnetized basement resembling that of oceanic crust,
122 extending the EBSB oceanic domain further NW than previously inferred from wide-angle data
123 (Fig. 2A). Gravity modeling also supports a more extended oceanic domain, with boundaries
124 comparable to our results (Graham et al., 2013) (Fig. DR1B).
125 Crustal thickness and velocity structure are usually reliable parameters to discriminate crustal
126 composition in extensional settings (e.g., Prada et al., 2014). However, observations from wide-
127 angle data and magnetic anomaly modeling suggest contradicting results on crustal distribution
128 in the EBSB. Below we explain this apparent contradiction based on the tectono-magmatic
129 evolution of the EBSB.

130 **2.2. Tectono-Magmatic Evolution**

131 The EBSB rotational opening resulted in a V-shaped basin with increased extension to the SE
132 (Okay et al., 1994; Shillington et al., 2008). Analytical and numerical models of V-shaped basins

show that, as rifting propagates, stretching increases with distance from the pole of rotation and breakup initiates away from the pole, propagating towards it and into stretched continental lithosphere (e.g., Vink, 1982; Le Pourhiet et al., 2018). As spreading progresses, spatial and temporal variations in magmatic crustal accretion driven by mantle temperature, strain localization, and spreading rates, can influence the emplaced crustal structure and its geophysical character (Franke, 2013). Changes in crustal structure within Domain III may reflect along-axis changes in magmatism (e.g., Muller et al., 1999; Hooft et al., 2000), and/or variations in melt supply over time (e.g., Tucholke et al., 1997; Cannat et al., 2003). Such changes would mainly cause variations in oceanic Layer 3 thickness (e.g., Mutter and Mutter, 1993; Grevemeyer et al., 2018). Oceanic Layer 2, characterized by lower seismic velocities (e.g., Mutter and Mutter, 1993) and considered to be the main source of oceanic magnetic anomalies (e.g., Talwani et al., 1971), would not be much affected. An enhanced melt supply, driven by the advection of warm asthenosphere during lithospheric thinning or by the presence of a hot mantle plume (e.g., Hopper et al., 2003), can form atypically thick oceanic crust with a well-developed, high-velocity Layer 3. Lower melt supply, due to an initially cool lithosphere or conductive cooling at slow extension rates suppressing partial melting (Bown and White, 1995), will result in a thinner oceanic crust mostly characterized by Layer 2 velocities. Models of rotational basin opening suggest that a decrease in extension rates toward the rotational pole results in an along-axis reduction in the volumes of decompression melt (Franke, 2013), but do not explain the abrupt change in crustal structure at the OPf (Fig. 2A, yellow line, Fig. 4).

Discontinuities and/or transform faults can control magma supply along spreading segments (e.g., Fox and Gallo, 1984; Georgen and Lin, 2003), and thermal perturbation by transforms often results in a reduction in crustal thickness near the transforms (e.g., Hooft et al., 2000),

156 resulting in anomalous oceanic crustal structure (e.g., Dunn and Martinez, 2011). Numerical
157 models show that transfer/transform faults can act as rift propagation barriers delaying the
158 opening of consecutive rift segments (Koopmann et al., 2014). Rift delay can affect both mantle
159 and melt flow between segments, limiting the propagation of low-viscosity mantle across the
160 segment boundary, and favoring melt accumulation at the opening segment (Koopmann et al.,
161 2014). The model predicts rift-parallel flow and concomitant magmatic peaks near the
162 propagation barrier caused by the lateral pressure gradient between sequentially opening
163 segments. This flow may result in abrupt changes in crustal thickness at segment boundaries
164 matching observations from the EBSB. Thus, the OPf may have acted as a rift propagation
165 barrier between SE and NW segments, resulting in pooling of melt to the SE. Such a model
166 would explain the abrupt transition from a thick oceanic crust SE of the OPf, with a well-
167 developed Layer 3, and thin oceanic crust NW of the OPf, with a thin/absent Layer 3, velocities
168 similar to those of thinned continental crust, but still with a distinctive magnetic character (Fig.
169 4).
170 Based on these considerations, we propose that the observed variations in crustal thickness and
171 lower-crustal velocities in Domain III result from changes in oceanic crustal accretion rather than
172 a change in crustal type. Variations in magma supply driven by the geometry of the opening rift,
173 and the effect of segmentation, were major controls on the basin architecture and the crustal
174 structure at the newly emplaced EBSB crust.

CONCLUSIONS

Based on basement morphology and magnetization, we have drawn new boundaries for the oceanic crust in the EBSB. Changes in crustal thickness and velocity structure from wide-angle seismic data within this oceanic domain, previously interpreted to show oceanic crust only to the very SE, are interpreted instead as evidence for changes in magma supply during spreading. Rift segmentation and transform faults may have played an important role in controlling the along-axis flow of mantle and melt. Initial spreading focused in the wider SE rift segment, where enhanced decompression melting and melt pooling caused the emplacement of thick oceanic crust with a well-developed Layer 3. Melt propagation to the NW was limited by transform faults, particularly the OPf, and/or by rift narrowing suppressing partial melting, resulting in the emplacement of a thinner oceanic crust lacking a well-developed Layer 3.

This study highlights the ambiguity in the geophysical characterization of crustal type and distribution in rifted margin settings. Although large amount of data are often available, different and perhaps contradicting interpretations are possible, especially where geophysical evidence deviates from what is “normally” expected for continental and oceanic crusts. In such cases, to avoid contradicting interpretations, data comparison and integration is essential.

ACKNOWLEDGMENTS

We thank Sasha Brune and Tiago Alves for constructive comments that improved the paper. We thank Geology Without Limits (GWL) for making the seismic dataset available to us. We are grateful to GWL for permission to show their confidential seismic sections. Parties interested in acquiring these data and corresponding data reports can contact the vendors through their websites at www.gwl-geo.com. We thank Schlumberger for providing the Petrel software that

was used for seismic display, interpretation and depth conversion. Also, we thank Geosoft for providing Oasis Montaj software used for the magnetic anomaly modeling. The EMAG2v3, from where we extracted the anomaly data for the EBSB region, is available at https://www.ngdc.noaa.gov/geomag/emag2.html or https://doi.org/10.7289/V5H70CVX. VM was supported by NERC Centre for Doctoral Training (CDT) in Oil and Gas. TAM was supported by a Wolfson Research Merit Award.

REFERENCES CITED

Ball, P., Eagles, G., Ebinger, C., McClay, K., and Totterdell, J., 2013, The spatial and temporal evolution of strain during the separation of Australia and Antarctica. Geochemistry, Geophysics, Geosystems, 14(8), 2771-2799. doi: 10.1002/ggge.20160

Bown, J. W., and White, R. S., 1995, Effect of finite extension rate on melt generation at rifted continental margins. Journal of Geophysical Research: Solid Earth, 100(B9), 18011-18029. https://doi.org/10.1029/94JB01478

Cannat, M., Rommevaux-Jestin, C., and Fujimoto, H., 2003, Melt supply variations to a magma-poor ultra-slow spreading ridge (Southwest Indian Ridge 61° to 69° E). Geochemistry, Geophysics, Geosystems, 4(8). doi:10.1029/2002GC000480

Dunn, R. A., and Martinez, F., 2011, Contrasting crustal production and rapid mantle transitions beneath back-arc ridges. Nature, 469(7329), 198. doi:10.1038/nature09690

Finetti, I., Bricchi, G., Del Ben, A., Pipan, M., and Xuan, X., 1988, Geophysical study of the Black Sea area. Bollettino di Geofisica Teorica e Applicata, 30(117), 197-324.

Fox, P. J., and Gallo, D. G., 1984, A tectonic model for ridge-transform-ridge plate boundaries: Implications for the structure of oceanic lithosphere. Tectonophysics, 104(3-4), 205-242. https://doi.org/10.1016/0040-1951(84)90124-0

Franke, D., 2013, Rifting, lithosphere breakup and volcanism: Comparison of magma-poor and volcanic rifted margins. Marine and Petroleum geology, 43, 63-87. http://dx.doi.org/10.1016/j.marpetgeo.2012.11.003

Georgen, J. E., and Lin, J., 2003, Plume-transform interactions at ultra-slow spreading ridges: Implications for the Southwest Indian Ridge. Geochemistry, Geophysics, Geosystems, 4(9). doi:10.1029/2003GC000542

Graham, R., Kaymakci, N., and Horn, B. W., 2013, The Black Sea: something different. Geo Expro, 10(5), 57-62.

Grevemeyer, I., Ranero, C. R., and Ivandic, M., 2018, Structure of oceanic crust and serpentinization at subduction trenches. Geosphere, 14(2), 395-418. doi:10.1130/GES01537.1

Haupert, I., Manatschal, G., Decarlis, A., and Unternehr, P., 2016, Upper-plate magma-poor rifted margins: Stratigraphic architecture and structural evolution. Marine and Petroleum Geology, 69, 241-261. http://dx.doi.org/10.1016/j.marpetgeo.2015.10.020

Hooft, E. E. E., Detrick, R. S., Toomey, D. R., Collins, J. A., and Lin, J., 2000, Crustal thickness and structure along three contrasting spreading segments of the Mid-Atlantic Ridge, 33.5–35 N. Journal of Geophysical Research: Solid Earth, 105(B4), 8205-8226. https://doi.org/10.1029/1999JB900442

Hopper, J. R., Dahl-Jensen, T., Holbrook, W. S., Larsen, H. C., Lizarralde, D., Korenaga, J., Kent, G., M., and Kelemen, P. B., 2003, Structure of the SE Greenland margin from seismic reflection and refraction data: Implications for nascent spreading center subsidence and asymmetric crustal accretion during North Atlantic opening. Journal of Geophysical Research: Solid Earth, 108(B5). doi:10.1029/2002JB001996

244 Kazmin, V. G., Shreider, A. A., and Shreider, A. A., 2007, Age of the western Black Sea basin
245 according to an analysis of the anomalous magnetic field and geological data. Oceanology,
246 47(4), 571-578. doi:10.1134/S0001437007040145
247 Koopmann, H., Brune, S., Franke, D., and Breuer, S., 2014, Linking rift propagation barriers to
248 excess magmatism at volcanic rifted margins. Geology, 42(12), 1071-1074.
249 doi:10.1130/G36085.1
250 Le Pourhiet, L., Chamot-Rooke, N., Delescluse, M., May, D. A., Watremez, L., and Pubellier,
251 M., 2018, Continental break-up of the South China Sea stalled by far-field compression.
252 Nature Geoscience, 11(8), 605. https://doi.org/10.1038/s41561-018-0178-5
253 Malinverno, A., 1991, Inverse square-root dependence of mid-ocean-ridge flank roughness on
254 spreading rate. Nature, 352(6330), 58.
255 Meyer, B., Saltus, R., and Chulliat, A., 2017, EMAG2: Earth Magnetic Anomaly Grid (2-arc-
256 minute resolution) Version 3. National Centers for Environmental Information, NOAA.
257 Model. doi:10.7289/V5H70CVX
258 Monteleone, V., Minshull, T. A., and Marin-Moreno, H., 2019, Spatial and temporal evolution of
259 rifting and continental breakup in the Eastern Black Sea Basin revealed by long-offset
260 seismic reflection data. Tectonics, 38. https://doi.org/10.1029/2019TC005523
261 Muller, M. R., Minshull, T. A., and White, R. S., 1999, Segmentation and melt supply at the
262 Southwest Indian Ridge. Geology, 27(10), 867-870. https://doi.org/10.1130/0091-
263 7613(1999)027<0867:SAMSAT>2.3.CO;2
264 Mutter, C. Z., and Mutter, J. C., 1993 Variations in thickness of layer 3 dominate oceanic crustal
265 structure. Earth and Planetary Science Letters, 117(1-2), 295-317.
266 https://doi.org/10.1016/0012-821X(93)90134-U

267 Nikishin, A. M., Okay, A. I., Tüysüz, O., Demirer, A., Amelin, N., and Petrov, E., 2015, The
268 Black Sea basins structure and history: New model based on new deep penetration regional
269 seismic data. Part 1: Basins structure and fill. Marine and Petroleum Geology, 59, 638-655.
270 https://doi.org/10.1016/j.marpetgeo.2014.08.017
271 Okay, A. I., Celal Sengor, A. M., and Görür, N., 1994, Kinematic history of the opening of the
272 Black Sea and its effect on the surrounding regions. Geology, 22(3), 267-270.
273 https://doi.org/10.1130/0091-7613(1994)022<0267:KHOTOO>2.3.CO;2
274 Pickup, S. L. B., Whitmarsh, R. B., Fowler, C. M. R., and Reston, T. J., 1996, Insight into the
275 nature of the ocean-continent transition off West Iberia from a deep multichannel seismic
276 reflection profile. Geology, 24(12), 1079-1082. https://doi.org/10.1130/0091-
277 7613(1996)024<1079:IITNOT>2.3.CO;2
278 Prada, M., Sallarès, V., Ranero, C. R., Vendrell, M. G., Grevemeyer, I., Zitellini, N., and de
279 Franco, R., 2014, Seismic structure of the Central Tyrrhenian basin: Geophysical constraints
280 on the nature of the main crustal domains. Journal of Geophysical Research: Solid Earth,
281 119(1), 52-70. https://doi.org/10.1002/2013JB010527
282 Sauter, D., Tugend, J., Gillard, M., Nirrengarten, M., Autin, J., Manatschal, G., Cannat, M.,
283 Leroy, S. and Schaming, M., 2018, Oceanic basement roughness alongside magma-poor
284 rifted margins: insight into initial seafloor spreading. Geophysical Journal International,
285 212(2), 900-915. doi: 10.1093/gji/ggx439
286 Searle, R. C., et al., 2010, Structure and development of an axial volcanic ridge: Mid-Atlantic
287 Ridge, 45 N. Earth and Planetary Science Letters, 299(1-2), 228-241.
288 doi:10.1016/j.epsl.2010.09.003

289 Shillington, D. J., Scott, C. L., Minshull, T. A., Edwards, R. A., Brown, P. J., and White, N.,
290 2009, Abrupt transition from magma-starved to magma-rich rifting in the eastern Black Sea.
291 Geology, 37(1), 7-10. doi: 10.1130/G25302A
292 Shillington, D. J., White, N., Minshull, T. A., Edwards, G. R., Jones, S. M., Edwards, R. A., and
293 Scott, C. L., 2008, Cenozoic evolution of the eastern Black Sea: A test of depth-dependent
294 stretching models. Earth and Planetary Science Letters, 265(3-4), 360-378.
295 doi:10.1016/j.epsl.2007.10.033
296 Sibuet, J. C., Srivastava, S., and Manatschal, G., 2007, Exhumed mantle-forming transitional
297 crust in the Newfoundland-Iberia rift and associated magnetic anomalies. Journal of
298 Geophysical Research: Solid Earth, 112(B6). doi:10.1029/2005JB003856
299 Small, C., 1994, A global analysis of mid-ocean ridge axial topography. Geophysical Journal
300 International, 116(1), 64-84. https://doi.org/10.1111/j.1365-246X.1994.tb02128.x
301 Starostenko, V. I., Dolmaz, M. N., Kutas, R. I., Rusakov, O. M., Oksum, E., Hisarli, Z. M.,
302 Okyar, M., Kalyoncuoglu, U. Y., Tununsatar, H. E. and Legostaeva, O. V., 2014, Thermal
303 structure of the crust in the Black Sea: comparative analysis of magnetic and heat flow data.
304 Marine Geophysical Research, 35(4), 345-359. doi: 10.1007/s11001-014-9224-x
305 Starostenko, V. I., Rusakov, O. M., Pashkevich, I. K., Kutas, R. I., Makarenko, I. B., Legostaeva,
306 O. V., Lebed, T. V. and Savchenko, A., 2015, Heterogeneous structure of the lithosphere in
307 the Black Sea from a multidisciplinary analysis of geophysical fields. Geofizicheskiy
308 zhurnal, 37(2), 3-28.
309 Starostenko, V., et al., 2004, Topography of the crust–mantle boundary beneath the Black Sea
310 Basin. Tectonophysics, 381(1-4), 211-233. doi:10.1016/j.tecto.2002.08.001

311 Talwani, M., Windisch, C., and Langseth, M., 1971, Reykjanes ridge crest: A detailed
312 geophysical study, J. Geophys. Res., 76, 473-517.
313 Tari, G., et al., 2018, Stratigraphy, structure and petroleum exploration play types of the Rioni
314 Basin, Georgia. Geological Society, London, Special Publications, 464.
315 https://doi.org/10.1144/SP464.14
316 Tucholke, B. E., Lin, J., Kleinrock, M. C., Tivey, M. A., Reed, T. B., Goff, J., and Jaroslow, G.
317 E., 1997, Segmentation and crustal structure of the western Mid-Atlantic Ridge flank, 25°
318 25′–27° 10′ N and 0–29 my. Journal of Geophysical Research: Solid Earth, 102(B5), 10203-
319 10223. https://doi.org/10.1029/96JB03896
320 Tucholke, B. E., Sawyer, D. S., and Sibuet, J. C., 2007, Breakup of the Newfoundland–Iberia
321 rift. Geological Society, London, Special Publications, 282(1), 9-46. doi: 10.1144/SP282.2
322 Tugend, J., Manatschal, G., Kusznir, N. J., and Masini, E., 2015, Characterizing and identifying
323 structural domains at rifted continental margins: application to the Bay of Biscay margins
324 and its Western Pyrenean fossil remnants. Geological Society, London, Special Publications,
325 413(1), 171-203. http://doi.org/10.1144/SP413.3
326 Vink, G. E., 1982, Continental rifting and the implications for plate tectonic reconstructions.
327 Journal of Geophysical Research: Solid Earth, 87(B13), 10677-10688.
328 https://doi.org/10.1029/JB087iB13p10677
329 Zhao, F., Alves, T. M., Wu, S., Li, W., Huuse, M., Mi, L., Sun, Q., and Ma, B., 2016, Prolonged
330 post-rift magmatism on highly extended crust of divergent continental margins (Baiyun Sag,
331 South China Sea). Earth and Planetary Science Letters, 445, 79-91.
332 http://dx.doi.org/10.1016/j.epsl.2016.04.001

Zonenshain, L. P., and Le Pichon, X., 1986, Deep basins of the Black Sea and Caspian Sea as remnants of Mesozoic back-arc basins. Tectonophysics, 123(1-4), 181-211. https://doi.org/10.1016/0040-1951(86)90197-6

337 **FIGURE CAPTIONS**

338 Figure 1. Reduced-to-pole magnetic anomaly map (EMAG2-v3) for the EBSB region. Black
339 lines mark GWL seismic profiles. Prominent positive anomalies correspond to the Shatsky Ridge
340 (SR), the Mid Black Sea High (MBSH), the Eastern Pontides (EP) magmatic arc, and contrast
341 with the negative anomaly of the central basin.

342

343 Figure 2. Summary of the basement morphology and distribution across the EBSB based on
344 seismic interpretation. (A) Map of the identified crustal domains (Domain I, II and III). Overlain
345 on map, the location of the GWL profiles, of sections shown in (B)-(E), and of wide-angle
346 seismic profiles (Shillington et al., 2009). The color code for the wide-angle lines shows the
347 crustal distribution interpreted by Shillington et al. (2009). Volcanics (red stars) are identified
348 within Domain III (Nikishin et al., 2015). Transform faults interpreted in the SE of the basin are
349 named after Tari et al. (2018). To the SE, we have insufficient data to constrain the seismic
350 character in Domain III(?). (B) Domain I - tilted and faulted crustal blocks. (C) Domain II -
351 rough basement with no extensional faulting, nor syn-rift deposits. (D) Domain III - smooth
352 basement with no extensional faulting. (E) Domain III - smooth basement affected by high-angle
353 transform faults; the thick sub-vertical dashed line shows the location of the Ordu-Pitsuda fault
354 (OPf).

355

356 Figure 3. Magnetic anomaly modeling along profile bs-110 (location shown in Figs.1 and 2A).
357 Top panel displays the comparison between calculated (red line) and observed (black line)
358 anomalies. The root-mean-squared (RMS) error, expressed in nT, between observed and
359 calculated anomaly is shown at the bottom left corner. The grey band represents the anomaly

variations 15 km either side of the profile. Colored backgrounds show the lateral extent and intensity (dark - high intensity; pale - low intensity) of the magnetized layers: pink - continental domain; blue - oceanic crust. Bottom panel shows the model generating the calculated anomaly and the magnetization for each layer.

Figure 4. Conceptual 3D and 2D models for oceanic crustal accretion in the EBSB. After back-arc extension, breakup focused in the wider SE rift where higher amount of decompression melt and melt focusing favored the emplacement of a thick oceanic crust with a well-developed Layer 3 (L3). Some volcanics are also visible in this area, probably extruded along fracture zones separating different spreading segments. Transform faults, particularly the OPf, acted as barriers limiting melt propagation towards the NW. In this area, a reduced supply of decompression melt and a limited melt migration from the SE segment, caused the emplacement of a thinner oceanic crust characterized mostly by the upper oceanic Layer 2 (L2). The main geophysical difference between the SE and the NW oceanic domains is the change in oceanic crustal thickness and velocity structure, related to the absence/near absence of L3 along the NW segment.

[1]GSA Data Repository item 2019xxx, additional information on seismic data (Table DR1), magnetic anomaly data and methodology used in this study, together with a comparison between our and previous results on crustal distribution in the basin (Figure DR1), and additional magnetic anomaly modeling results (Figures DR2-8), is available online at http://www.geosociety.org/datarepository/2019/, or on request from editing@geosociety.org or Documents Secretary, GSA, P.O. Box 9140, Boulder, CO 80301, USA.

Figure 1

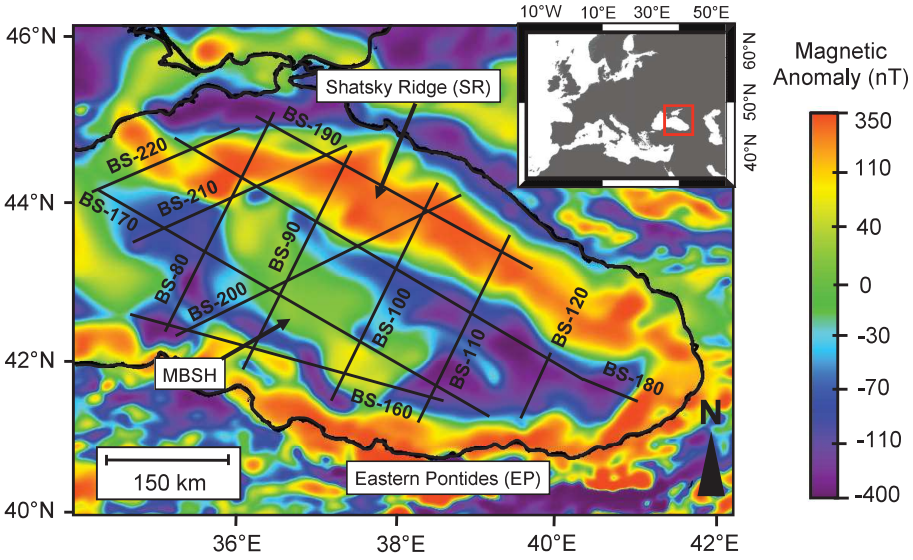
10°W
10°E
30°E
50°E
60°N
50°N
40°N
46°N
44°N
42°N
40°N
36°E
38°E
40°E
42°E
Shatsky Ridge (SR)
BS-190
BS-220
BS-210
BS-170
BS-90
BS-80
BS-200
BS-100
BS-110
BS-120
BS-180
BS-160
MBSH
150 km
Eastern Pontides (EP)
N
Magnetic Anomaly (nT)
350
110
40
0
-30
-70
-110
-400

Figure 2

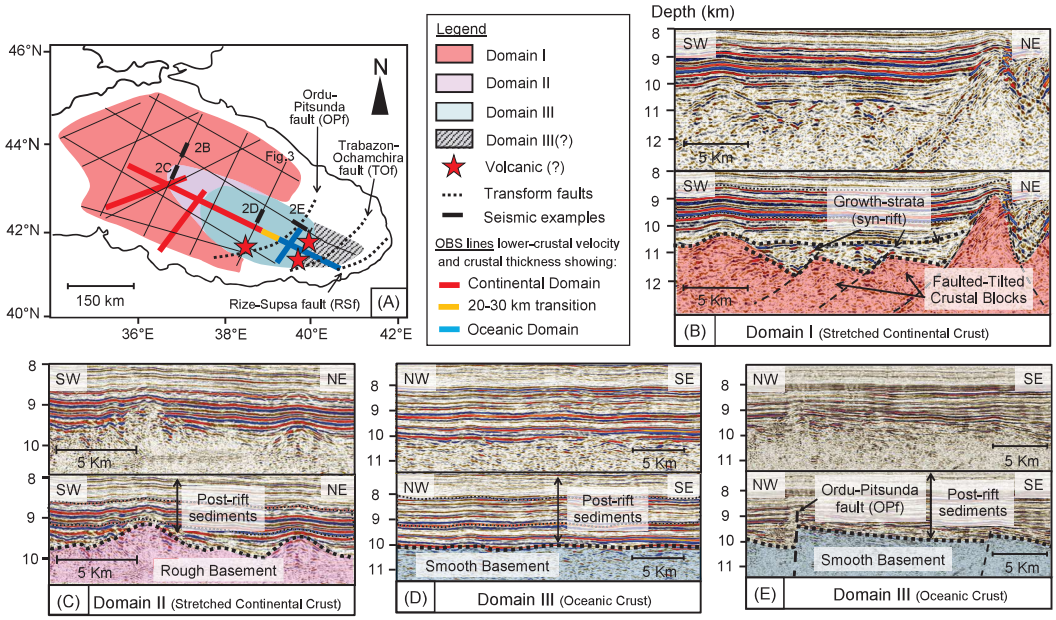
46°N
44°N
42°N
40°N
36°E
38°E
40°E
42°E
N
Ordu-Pitsunda fault (OPf)
Trabazon-Ochamchira fault (TOf)
Rize-Supsa fault (RSf)
Fig.3
2B
2C
2D
2E
150 km
(A)
Legend
Domain I
Domain II
Domain III
Domain III(?)
Volcanic (?)
Transform faults
Seismic examples
OBS lines lower-crustal velocity and crustal thickness showing:
Continental Domain
20-30 km transition
Oceanic Domain
Depth (km)
SW
NE
5 Km
Growth-strata (syn-rift)
Faulted-Tilted Crustal Blocks
(B) Domain I (Stretched Continental Crust)
Post-rift sediments
Rough Basement
(C) Domain II (Stretched Continental Crust)
NW
SE
Smooth Basement
(D) Domain III (Oceanic Crust)
Ordu-Pitsunda fault (OPf)
(E) Domain III (Oceanic Crust)

Figure 3

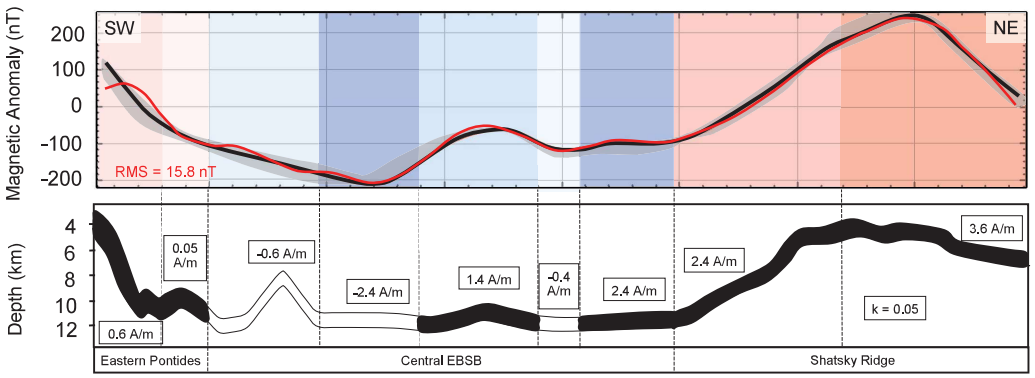
Magnetic Anomaly (nT)
200
100
0
-100
-200
SW
NE
RMS = 15.8 nT
Depth (km)
4
6
8
10
12
0.05 A/m
-0.6 A/m
-2.4 A/m
1.4 A/m
-0.4 A/m
2.4 A/m
2.4 A/m
3.6 A/m
0.6 A/m
k = 0.05
Eastern Pontides
Central EBSB
Shatsky Ridge

Figure 4

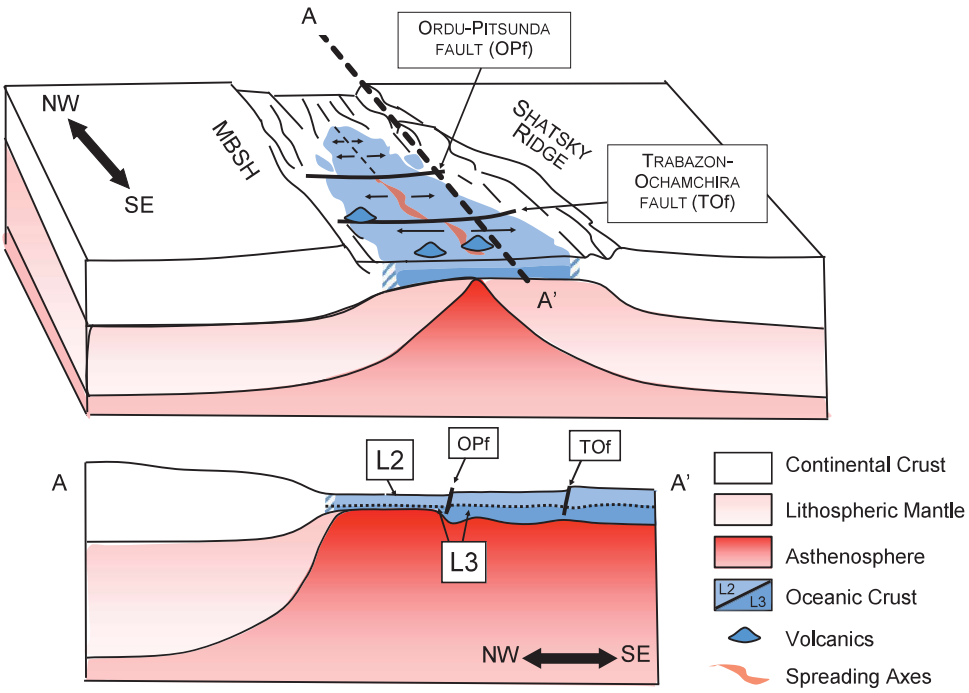
A
ORDU-PITSUNDA FAULT (OPf)
NW
SE
MBSH
SHATSKY RIDGE
TRABAZON-OCHAMCHIRA FAULT (TOf)
A'
A
L2
OPf
TOf
A'
L3
NW
SE
Continental Crust
Lithospheric Mantle
Asthenosphere
L2
L3
Oceanic Crust
Volcanics
Spreading Axes